Spectroscopic ellipsometry study of barrier width effect in self-organized InGaAs/GaAs QDs laser diodes

M S Al-Ghamdi[a], A Sayari[b,c*] & L Sfaxi[d,e]

[a]Department of Physics, Faculty of Science, King Abdulaziz University, P.O. Box 80203, Jeddah 21589, Saudi Arabia

[b]Department of Physics, Faculty of Science, University of Jeddah, P.O. Box 80327, Jeddah 21589, Saudi Arabia

[c]Université de Tunis El Manar, Faculté des Sciences de Tunis, Unité de recherche Spectroscopie Raman UR13ES31, 2092, Tunis, Tunisie

[d]Laboratoire de Micro-Optoélectroniques et Nanostructures, Université de Monastir, Tunisie

[e]High School of Sciences and Technology of Hammam Sousse, Université de Sousse, Tunisie

Molecular beam epitaxy (MBE) is used to grow InGaAs/GaAs quantum dots (QDs) laser diodes (LDs) with different barrier widths (5, 10 and 15 nm) at 580 ℃ on GaAs substrates. Optical properties of the InGaAs/GaAs QDs LDs have been investigated by using the spectroscopic ellipsometry (SE) technique. A general oscillator optical model has been utilized to fit the experimental data in order to obtain the LD layer thicknesses, refractive index and absorption coefficient. The dielectric function, the energy band gap and the surface and volume energy loss functions are computed in the energy range 1-6 eV. The optical properties of the deposited InGaAs/GaAs QDs LDs are found to be affected by the barrier width, which give more insight into carriers dynamics and optical parameters in these devices. The refractive indices, the extinction coefficients and the dielectric constants of the LDs with barrier widths 15 and 10 nm are relatively larger than those of the LD with barrier width 5 nm. These indicate that optical properties of LDs with larger barrier widths (15 and 10 nm) will be improved. The interband transition energies in the three devices have calculated and identified. Two energy gaps at 1.04 and ~1.37 eV are obtained for all the heterostructures which indicates that fabricated LDs may be operating for a wavelength of 1.23 μm at room temperature.

Keywords: Semiconductor laser diode, Quantum dot, Molecular beam epitaxy, Arsenides, Dielectric function, Ellipsometry

1 Introduction

Semiconductor laser diodes (LDs) are highly desired for applications including optical communication, digital data storage, printing, material processing and display technology. LDs emitting in the wavelength range 1.25-1.65 μm are important for a variety of applications particularly, optical amplifiers for optical data- and telecommunication[1-4]. The nanotechnology progress has led to the development of quantum dot (QD) LDs which have improved performance compared to bulk, QW or quantum wire LDs. Theoretical and experimental studies demonstrated that QD lasers have many advantages such that low power consumption, high-speed operation, and large modulation bandwidth[5,6]. However, the modal gain of QD systems is generally lower than quantum well structures which is why QD lasers have long cavities. Also, the threshold current density for QD lasers is stable only in some very special circumstances in a limited temperature range.

The threshold current instability in QD lasers is due to inhomogeneous broadening and carrier loss to excited states and the wetting layer. While the inhomogeneous broadening in an ensemble of dots is interesting for short-pulse generation. The 0.9-1.4 μm emission wavelengths range of InAs/GaAs QDs[7] allowed the performance development of optoelectronic devices for fiber telecommunications[8] and consumer electronics[9-11].

The output power of QD lasers depends on many parameters such as the surface density of QDs, the QD uniformity and the number of QD sheets. Therefore, high-density, highly-uniform and multi-stacked QDs will lead to a large optical gain. There are many previous studies focused on high-gain GaAs-based QD lasers in the 1-1.3 μm emission wavelengths range[12-15]. However, problems remain in the growth techniques and the lack of uniformity in QD size, limiting the performance of these lasers below the theoretically predicted values. Also, other problems are appeared such as thermal escape of carriers from QDs to the wetting layer and barrier

---

*Corresponding Author (E-mail: amor.sayari@laposte.net)

states and gain saturation in the active region. The gain saturation issues can be resolved by raising the gain volume in the QD active region by stacking large number of QDs sheets[16]. However, the thermal escape of charge carriers can be minimized by using barriers with large bandgap such as GaAs surrounding the narrow gap InGaAs QD material. These lasers showed an increase in the differential efficiency and a reduction of the threshold current densities[17]. Barrier height is regarded as one of the most important parameters that affects the distribution of carriers upon the active region, and consequently reduces the threshold current density and increases the optical output power when optimized[18,19].

The barrier width effect on carrier distribution is another important issue in the design of a laser structure. Studies carried out in the past showed that uniformity of carriers increases with decreasing barrier thickness and considerable difference in the optical gain spectrum for two different barrier widths was obtained for the same carrier injection[20]. In addition, the location of the gain peak for the thin barrier was slightly shifted to a longer wavelength in comparison to a wide barrier structure, suggesting barrier thickness, to some extent, affects the laser emission wavelength. Therefore, barrier width may be considered as an addition parameter, beside well width and barrier height, for wavelength tuning.

In this work, we study the optical properties of three InGaAs/GaAs QDs LD structures grown by MBE at 580 °C on n$^+$-type GaAs substrates with different barrier widths. The active region of the investigated InGaAs/GaAs QDs LDs is composed of seven stacks InGaAs/GaAs QD heterostructure sandwiched by 50 nm $Al_{0.15}Ga_{0.85}As$ confining layer. The InGaAs QD layer has a thickness of 2.1 nm and the GaAs barrier layer has a thickness varying from 5 to 15 nm. The optical constants, energy gaps and the surface and volume energy loss functions of the three devices were obtained from spectroscopic ellipsometry (SE) data in the 1-6 eV photon energy range. The complex dielectric function is utilized to determine the higher order transitions and free carrier absorption. The effect of the barrier width on the optical properties of the InGaAs/GaAs QDs LDs has been investigated.

2 Experimental Details
2.1 Structure of the devices

The layered structure of the InGaAs/GaAs QDs LDs with various barrier layer thickness, shown

schematically in Fig. 1, was deposited by solid-source MBE on an n$^+$-doped GaAs (100) substrate at 580 °C. After initial oxide desorption, an n$^+$-type (10^{19} cm^{-3}) 0.5 µm thick GaAs buffer layer was grown. Following this, a 1.2 µm thick n-type (5×10^{18} cm^{-3}) $Al_{0.5}Ga_{0.5}As$ lower cladding layer, a laser active region surrounded by two 50 nm thin $Al_{0.15}Ga_{0.85}As$ confining layers, a 1.2 µm p-type (5×10^{18} cm^{-3}) upper cladding layer, and a p-doped (5×10^{18} cm^{-3}) 300 nm thick GaAs cap for ohmic contact, were deposited. During the deposition of the active region the substrate temperature is cooled down and stabilized to 500 °C to avoid segregation problems and indium desorption. The active region is composed of seven stacks InGaAs/GaAs QD heterostructure. The InGaAs QD layer has a thickness of 2.1 nm and the GaAs barrier layer thickness varies from 5 to 15 nm. The InGaAs QDs were formed following the Stranski-Krastanov growth mode[21]. This deposition procedure gives QDs ensemble with relatively high density (~5×10^{10} cm^{-2}) as reported by previous studies[22]. The growth rates of InAs and GaAs, measured by RHEED, were 0.25 Å/s during deposition of the $In_{0.5}Ga_{0.5}As$ QD layer. However, growth rate of 1.5 Å/s was used to grow the GaAs barrier layers. The growth velocities of GaAs and AlAs when deposing $Al_{0.15}Ga_{0.85}As$ confining layers were, respectively, 1.5 and 0.26 Å/s, whereas these velocities were equal to 1.5 Å/s when growing $Al_{0.5}Ga_{0.5}As$ cladding layers. Silicon (Si) and
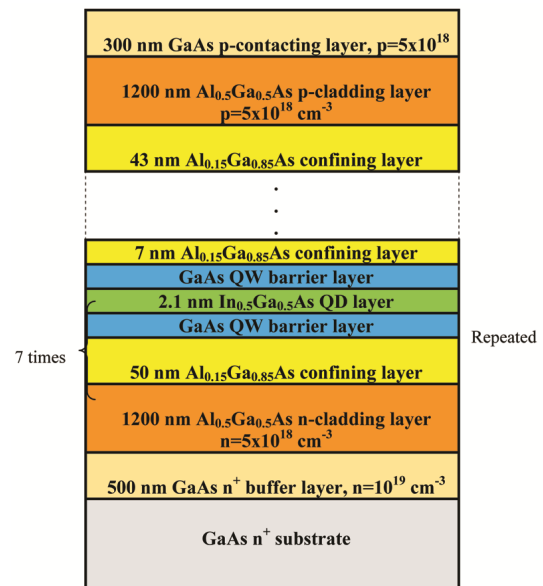

Fig. 1 – Diagram structure of the InGaAs/GaAs QD LDs grown on GaAs substrates with different barrier widths.

Beryllium (Be) were used as n- and p-type dopants, respectively.

2.2 Characterization technique

SE experiments were carried out using a J A Woollam Variable Angle Spectroscopic Ellipsometer (VASE) M-2000 model. VASE is a rotating compensator ellipsometer equipped with an auto-retarder, which is useful in measuring the depolarization caused by the surface roughness, substrate reflection, and thickness non-uniformity. This system incorporates a CCD spectrometer for simultaneous spectral readout from 1 to 6 eV.

Ellipsometric measurements are typically reported in terms of phase difference between components of light polarized parallel (E_p) and perpendicular (E_s) to the plane of incidence, Δ, and the change in the ratio of their amplitudes ($\frac{r_p}{r_s}$) given by tanΨ. The resulting change in polarization after reflection from a sample surface can be measured through the complex reflection coefficient, $\rho = \frac{r_p}{r_s} = tan\psi e^{i\Delta}$ [23,24]. To extract useful information from VASE data, optical models for GaAs substrate, LD layers, and surface roughness were constructed using a software package complete EASE (ver. 4.29, 2009) by J. A. Woollam Co., Inc. The comparison between generated (modeled) and experimental results is made through a fitting procedure. A good model is constructed from the chemical and physical histories of a system in which differences between the chosen model and experimental data are minimal. The mean-squared error (MSE) is the quality estimator of parameters as a sum of squares of differences between modeled and measured data. To qualify the fitting, a Lavenberg-Marquardt regression algorithm was used to obtain lowest value of MSE[25-28]. In the model, the surface roughness layer is formed of a mixture of Cauchy dispersion and 50% of voids or air. The SE experiments were performed at 300 K in the 1-6 eV energy region, with angle of incidence ϕ varying from 50 to 70°.

3 Results and Discussion
3.1 Ellipsometry investigations

The proposed model to fit the ellipsometric data for the three samples is composed of the multilayer structure built up with 34-layers of the LD, the GaAs substrate and the top roughness layer. The General Oscillator ellipsometry model was applied to determine the optical constants. The model used in this study combines 5 Tauc-Lorentz oscillators to fit the experimental data. An example of the fit for the sample with barrier width 15 nm is shown in Fig. 2. It is clear from Fig. 2 that the data generated by the optical model fit well the experimental results in the 1-6 eV energy range. In general, for simple samples, like single thin films, a small value of the MSE (~1) is required for the acceptability of a model fit. For more complex structures (with thick and/or multiple layers) an MSE < 10 is still be considered acceptable[29,30]. The MSE values obtained for the three samples with barrier widths 5, 10 and 15 nm were, respectively, 5.27, 4.16 and 4.64. The ψ peaks in Fig. 2 (a) are attributed to excitonic absorption at ~3 and 5 eV. Ellipsometric spectra reveal oscillations at low energy originating from multiple reflections within the multi-layer interfaces of the InGaAs/GaAs QDs LDs.
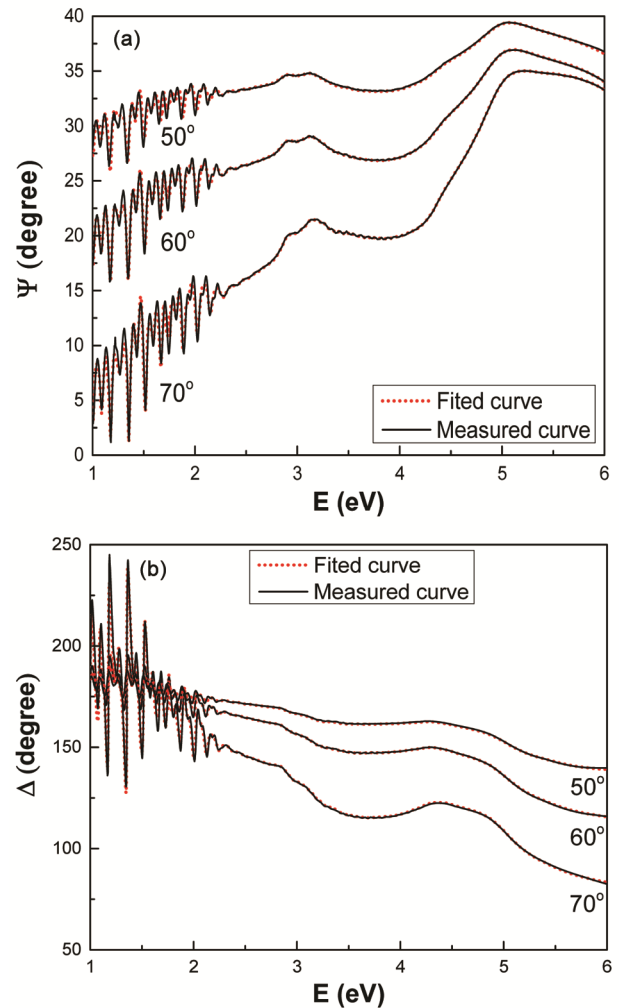

Fig. 2 – Room temperature SE spectra of ψ (a) and Δ (b) for the structure with barrier width 15 nm. The data generated by the optical model (dots) fit well the experimental results.

The refractive indices (n) and extinction coefficients (k) spectra of the three structures, deduced from the generated data, are shown in Fig. 3. The three k-spectra have the same behavior in all the 1-6 eV range. As the photon energy (E) increases, k increases in accordance with the Kramers-Kronig relations and the first maximum is seen at ~3 eV. Then, k decreases until ~4 eV and increases again to reach a second maximum at ~4.5 eV and continue to increase to a third maximum at ~4.8 eV. For photon energy higher than 4.8 eV, k decreases. Three energy transitions from the valence to the conduction band can be seen, the first is in the energy region 2.8-3.4 eV, the second in the interval 4.4-4.6 eV and the third transition in the energy range 4.7-4.9 eV. We note that k values of the two LDs with barrier widths 15 and 10 nm are relatively larger than that of the sample with barrier width 5 nm, particularly for $E > 3$ eV. The refractive index of the samples firstly increases as E increases until it attains its maximum at ~2.2 eV and then decreases but having two relative maxima at 4.2 and 4.7 eV. Higher values of n are obtained in the IR-visible region (n = 3.3 - 4), and a large fundamental absorption edge is seen in the IR region of the n spectra of the three structures. However, in the visible region, n has a weak dependence on the photon energy. From Fig. 3, it is clear that refractive indices of samples with barrier widths 15 and 10 nm are larger than that of the sample with barrier width 5 nm. We expect that absorption and gain will be improved for devices with large barrier widths since absorption and gain are proportional to the extinction coefficient. We note that there is small difference between n and k spectra for the two devices with barrier widths 10 and 15 nm which indicates probably weak effect of barrier width when the thickness exceeds 10 nm.

Figure 4 shows the real (ε_1) and imaginary (ε_2) parts of the dielectric function of the complex structures at 300 K for the 1-6 eV energy range. The two parts follow different patterns but their values for the devices with larger barrier widths (15 and 10 nm) are relatively higher than those of the device with smaller barrier width (5 nm) in the major energy interval. However, for $E > 4.7$ eV, opposite effect is observed for ε_1 values. The principal spectral features are observed at ~3 eV and ~4.5 eV[31,32]. The interband transition energies are calculated from the zero crossing of the second derivative spectrum of ε_2. The second energy derivative spectra of the three samples

are shown in Fig. 5 and the obtained transition energies are summarized in Table 1. The energy values of ~1.9, ~4.5 and ~4.7 eV correspond, respectively, to the $E_0 + \Delta_0$, E_0' and E_2, interband
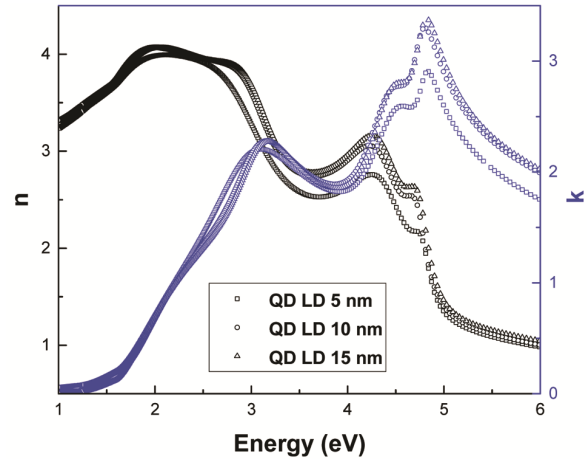

Fig. 3 – Refractive indices and extinction coefficients of the three complex structures grown with different barrier widths.
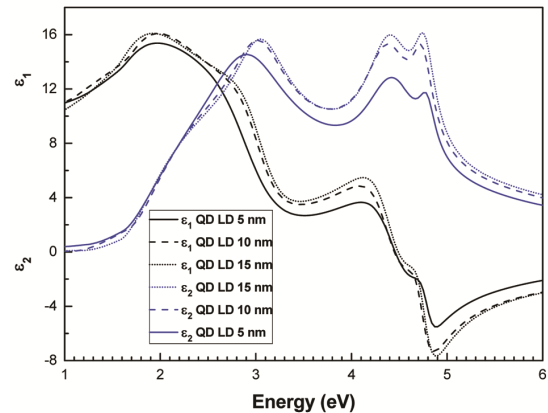

Fig. 4 – The ε_1 and ε_2 spectra of the three devices calculated from the generated data.
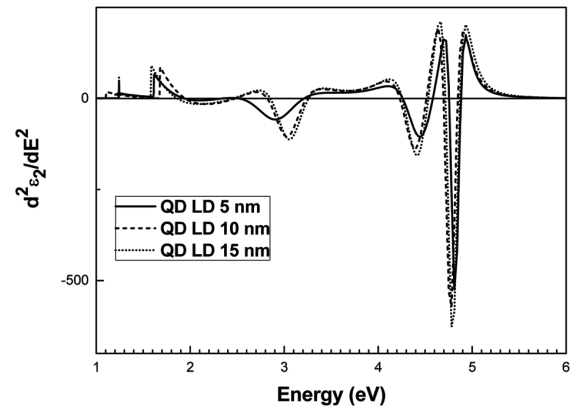

Fig. 5 – Second-derivative spectra of ε_2 as functions of photon energy for the three samples.

Table 1 – Comparison between the different CP energies obtained in our work and those of GaAs, AlGaAs and InGaAs at room temperature from[31-35].

CP Energy	E_0(eV)	$E_0+\Delta_0$(eV)	E_1(eV)	$E_1+\Delta_1$(eV)	E_0'(eV)	E_2(eV)	E_2'(eV)
QD LD 5	1.94	2.53	-	3.21	4.57	4.77	4.89
QD LD 10	1.95	2.48	2.82	3.24	4.52	4.71	4.86
QD LD 15	1.87	2.45	2.85	3.25	4.54	4.71	4.86
GaAs	1.42	1.75	2.91	3.14	4.45	4.77	-
$Al_{0.15}Ga_{0.85}As$	1.66	1.97	3.03	3.28	4.59	4.74	4.81
$Al_{0.5}Ga_{0.5}As$	2.08	2.37	3.26	3.49	4.66	4.75	4.82
$In_{0.5}Ga_{0.5}As$	0.75	1.15	2.57	3.6	4.45	4.84	-

transitions in $Al_{0.15}Ga_{0.85}As$ confining layers. However, the two energies at about 2.4 and 3.2 eV, are due to critical point (CP) transitions $E_0 + \Delta_0$, and E_1, respectively, in $Al_{0.5}Ga_{0.5}As$ cladding layers[32]. Also, Table 1 shows two interband transitions at ~2.8 and ~4.8 eV which correspond to the E_1 and E_2 CP energies of GaAs and $In_{0.5}Ga_{0.5}As$, respectively. We note that the contribution of the E_0' CP energy (4.6 eV) of $Al_{0.5}Ga_{0.5}As$[32] to the E_0' one of $Al_{0.15}Ga_{0.85}As$[31] cannot be neglected because the small energy difference between them. Similar remark concerns also the two nearly positioned E_2 interband transitions of the same layers (~4.7 eV). It is known that ϵ_2 is a gauge of material quality, the highest value implies the most abrupt interface[36]. The ϵ_2 spectra of samples with large barrier widths (10 and 15 nm) indicate the good quality of materials forming the devices grown by MBE. We note that there is no significant difference between ϵ_1 and ϵ_2 spectra for the two devices with larger barrier widths which indicates probably the weak effect of barrier width when thickness exceeds 10 nm.

The energy loss ratio for electrons crossing through a material is given by the surface and volume energy loss functions (SELF and VELF) and can be computed from ϵ_1 and ϵ_2 by $VELF = \frac{\epsilon_2}{\epsilon_1^2+\epsilon_2^2}$ and $SELF = \frac{\epsilon_2}{(1+\epsilon_1)^2+\epsilon_2^2}$ [37]. The changes with photon energy of both SELF and VELF of the structures are shown in Fig. 6. It is clear that SELF and VELF exhibit different behavior in the three energy regions 1-3 eV, 3-4.8 and 4.8-6 eV. In the first region (1-3 eV), SELF and VELF are nearly similar for the three devices. However, in the second region VELF values are larger than those of SELF for the three samples. Whereas, VELF and SELF of the LD with smaller barrier width (5 nm) are higher than those of LDs with larger barrier widths (10 and 15 nm). We note that SELF and VELF values of devices with larger
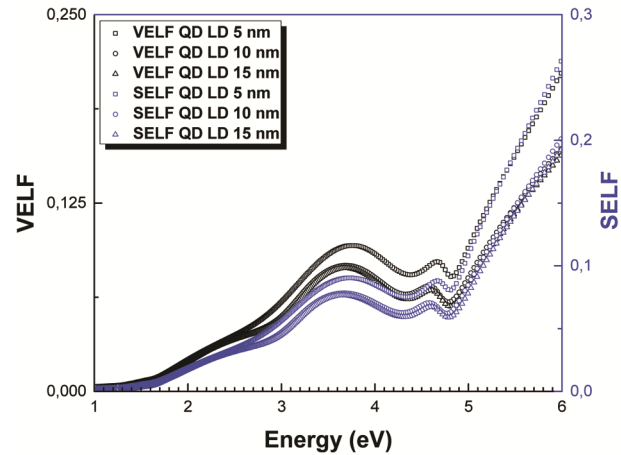

Fig. 6 – Energy loss functions (SELF and VELF) spectra of the three structures.

barrier widths are nearly similar in all the regions. This indicates that in the second region the principle energy loss arises in the volume of the three devices and more energy loss occurred in the LD with smaller barrier width. In the third region, the values of SELF are relatively larger than those of VELF for the three devices and have linear dependence with energy. SELF and VELF values of the device with smaller barrier width (5 nm) are larger than those of devices with larger barrier widths (10 and 15 nm). However, the energy loss in the third region arises in the surface of the InGaAs/GaAs QD LDs. Consequently, we can conclude that SELF and VELF of InGaAs/GaAs QDs LDs can be controlled by varying the LD barrier width.

3.2 Band structure and energy gap

InGaAs QDs represent confinement centers for charge carriers since the bandgap of InGaAs is lower than that of the surrounding materials GaAs and AlGaAs. The bandgap energy (E_g) of InGaAs-QDs is about 0.36 eV, inserted in larger bandgap GaAs layers with $E_g \approx 1.4$ eV, then a confining layer of
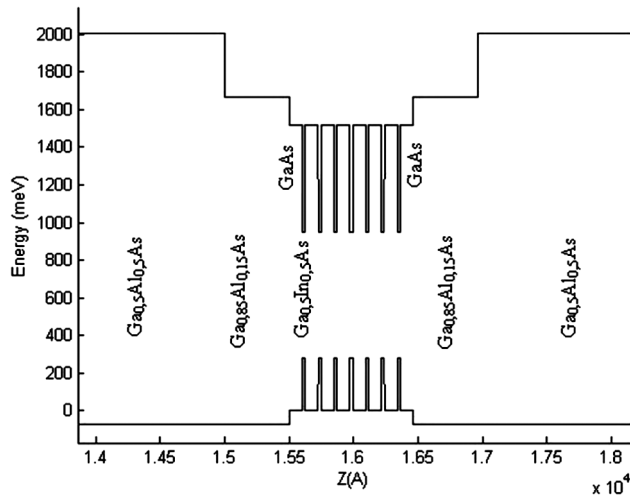
Fig. 7 – Energy difference diagram in the CB and VB for InGaAs/GaAs QD LD with barrier width 10 nm.
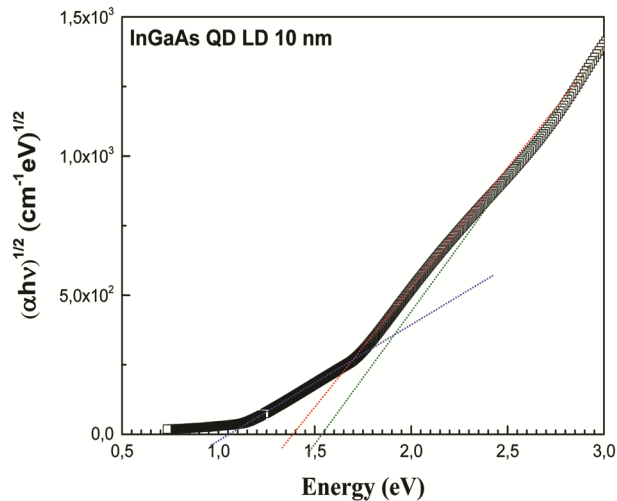

Fig. 8 –The $(\alpha E)^{1/2}$ versus E spectrum for the sample deposited with barrier width 10 nm.

Table 2 – Energy gaps of the three samples obtained from SE results at room temperature.

Sample	E_{g1}(eV)	E_{g2} (eV)	E_{g3} (eV)
QD LD 5	1.01	1.34	1.51
QD LD 10	1.04	1.37	1.58
QD LD 15	1.08	1.37	1.56

$Al_{0.15}Ga_{0.85}As$ with $E_g \approx 1.7$ eV then, cladding layers of $Al_{0.5}Ga_{0.5}As$ with $E_g \approx 2$ eV. The electrons and holes build up and population inversion formed in the QD active region caused by carrier confinement, and as a result, allows lasing. The energy diagram of the QDs LD with barrier width of 10 nm is shown in Fig. 7 as example. Band offset values between

GaInAs and GaAs and between GaAlAs and GaAs have been used in our calculations are taken from literature[38,39]. The origin of the energy is taken at the maximum of the valence band of GaAs.

In order to determine the E_g values of the structures, we calculated from the SE measurements the absorption coefficient ($\alpha = 4\pi k/\lambda$) and $(\alpha h\nu)^{1/2}$, since $In_xGa_{1-x}As$ material has an indirect band gap (for all x). Figure 8 shows the variation of $(\alpha h\nu)^{1/2}$ as function of E for the sample with barrier width 10 nm as example. The values of E_g obtained for the three devices are given in Table 2. The two values 1.04 and ~1.37 eV, obtained for all the structures, were attributed, respectively, to the fundamental and excited transitions in InGaAs QDs[40,41]. However, the value ~1.56 eV corresponds to the energy gap of AlGaAs[40]. We note that the small difference between fundamental and excited transition energies of InGaAs QDs (table 2) for the three samples can be related to the barrier width variation in the devices.

4 Conclusions

Three InGaAs/GaAs QDs LD structures, with various barrier widths of 5, 10 and 15 nm, were prepared with high quality on GaAs substrates by MBE at 580 °C. In order to obtain the optical constants as functions of E ranging from 1 to 6 eV at room temperature, a General Oscillator optical model was utilized to fit the experimental data. The optical properties of the deposited InGaAs/GaAs QDs LDs are found to be affected by the barrier width, particularly in the barrier width range 5-15 nm. We showed that computed energy loss functions can be controlled by varying the LD barrier width. SE data demonstrate that the barrier width is an important parameter in the design of InGaAs/GaAs QDs LD structures. We expect that absorption and gain will be improved for devices with large barrier widths (10 and 15 nm) since these devices have higher extinction coefficients. Therefore, we can conclude that optical properties of InGaAs/GaAs QDs LDs can be controlled by barrier width, which may help to improve the characteristics of these devices.

References

1 Bimberg D, *In proceedings of the 28th International Symposium on Compound Semiconductors*, (University of Tokyo), (2001) 485.

2 Sugawara M, Hatori N, Akiyama T, Nakata Y & Ishikawa H, *Jpn J Appl Phys*, 40 (2001) L488.

3 Tansu N, Yeh Y & Mawst L J, *Appl Phys Lett*, 82 (2003) 4038.

4 Asplund C, Sundgren P, Mogg S, Hammar M, Christiansson U, Oscarsson V, Runnstrm C, Odling E & Malmquist J, *Electron Lett*, 38 (2002) 635.

5 Asada M, Miyamoto Y & Suematsu Y, *IEEE J Quantum Electron*, 22 (1986) 1915.

6 Nahri D G, Arabshahi H & Abadi M R R, *Am J Phys*, 3 (2010) 138.

7 Goldstein L, Glas F, Marzin J Y, Charasse M N & Roux G L, *Appl Phys Lett*, 47 (1985) 1099.

8 Kageyama T, Nishi K, Yamaguchi M, Mochida R, Maeda Y, Takemasa K, Tanaka Y, Yamamoto T, Sugawara M & Arakawa Y, *Extremely High Temperature (220 °C) Continuous-Wave Operation of 1300-nm-Range Quantum-Dot Lasers*, (CLEO Europe, Munich: Germany), 2011.

9 Tanabe K, Watanabe K & Arakawa Y, *Appl Phys Lett*, 100 (2012) 192102.

10 Greenwood P D L, Childs D T D, Kennedy K, Groom K M, Hugues M, Hopkinson M, Hogg R A, Krstajic N, Smith L E, Matcher S J, Bonesi M, MacNeil S & Smallwood R, *IEEE J Select Top Quantum Electron*, 16 (2010) 1015.

11 Laser Q D, Inc (booth#4B25), 2009. [http://www.qdlaser.com/S].

12 Xu Z, Birkedal D, Juhl M & Hvam J M, *Appl Phys Lett*, 85 (2004) 3259.

13 Mi Z, Fathpour S & Bhattacharya P, *Electron Lett*, 41 (2005) 1282.

14 Amano T, Sugaya T, Komori K & Okada Y, *IEEE J Select Topi Quantum Electron*, 13 (2007) 1273.

15 Maximov M V, Ustinov V M, Zhukov A E, Kryzhanovskaya N V, Payusov A S, Novikov I I, Gordeev N Y, Shernyakov Y M, Krestnikov I, Livshits D, Mikhrin S & Kovsh A, *Semiconduct Sci Technol*, 23 (2008) 105004.

16 Schmidt O G, Kirstaedter N, Ledentsov N N, Mao M H, Bimberg D, Ustinov V M, Egorov A Y, Zhukov A E, Maximov M V, Kopev P S & Alferov Z I, *Electron Lett*, 32 (1996) 1302.

17 Zhukov A E, Ustino V M, Egorov A Y, Kovsh A R, Tatsulnikov A F, Maximov M V, Ledentsov N N, Zaitsev S V, Gordeev N Y, Kopchatov V I, Chernyakov Y M, Kopev P S, Bimberg D & Alferov Z I, *J Electron Mater*, 27 (1998) 106.

18 Hazell J F, Simmons J G, Evans J D & Blaauw C, *IEEE J Quantum Electron*, 34 (1998) 2358.

19 Hamp M J, Cassidy D T, Robinson B J, Zhao Q C, Thompson D A & Davies M, *IEEE Photon Technol Lett*, 10 (1998) 1380.

20 Hamp M J, Cassidy D T, Robinson B J, Zhao Q C & Thompson D A, *IEEE Photon Technol Lett*, 12 (2000) 134.

21 Daudin B, Widmann F, Feuillet G, Samson Y, Arlery M & Rouvière J L, *Phys Rev B*, 56 (1997) R7069.

22 Tokranov V E, Yakimov M, Katsnelson A, Dovidenko K, Todt R & Oktyabrsky S, *Proc SPIE*, 4656 (2002) 79.

23 Tompkins H G & Irene E A, *Handbook of Ellipsometry*, (William Andrew Publishing: Highland Mills), 2004.

24 Azzam R M A & Bashara N M, *Ellipsometry and Polarized Light*, (North-Holland Publ Co: Amsterdam), 1984.

25 Sayari A, El Mir L, Al-Heniti S, Al-Harbi T, Yaghmour S J & Al-Ghamdi A A, Eur Phy*s J Appl Phys*, 62 (2013) 30304.

26 Sayari A, El Mir L, Al-Heniti S, Shalaan E, Yaghmour S J, Al-Thabaiti S A, Al-Ghamdi A A & Yakuphanoglu F, *J Electroceram*, 30 (2013) 221.

27 Alyamani A, Sayari A, Albadri A, Albrithen H & El Mir L, *Eur Phys J Plus*, 131 (2016) 328.

28 Al-Ghamdi M S, Sayari A & Sfaxi L, *J Alloys Compd*, 685 (2016) 202.

29 Losurdo M & Hingerl K, *Ellipsometry at the Nanoscale*.pdf (2013).

30 Wollam J A, *Complete EASE™ Data Analysis Manual*, (Wollam Co Inc, Lincoln: NE), 2011.

31 Ozaki S & Adachi S, *J Appl Phys*, 78 (1995) 3380.

32 Kim T J, Yoon J J, Hwang S Y, Jung Y W, Ghong T H, Kim Y D, Kim H & Chang Y C, *Appl Phys Lett*, 97 (2010) 171912.

33 Kim C C, Garland J W & Raccah P M, *Phys Rev B*, 47 (1993) 1876.

34 Adachi S, Capper P, Kasap S & Willoughby A, *Properties of Group-IV, III-V and II-VI Semiconductors*, (John Wiley), 2005.

35 *Ihn Y S, Ghong T H, Kim Y D, Kim S J, Aspnes D E, Yao T & Koo B H, J Korean Phys Soc, 42 (2003) 242.*

36 *Aspnes D E & Studna A A, Appl Phys Lett, 39 (1981) 316.*

37 *Ritchie R H, Phys Rev, 106 (1957) 874.*

38 Saxena A K, *Solid State Commun*, 113 (2000) 201.

39 Goldberg Y A, Schmidt N M, Levinshtein M, Rumyantsev S & Shur M, *Handbook Series on Semiconductor Parameters*, (World Scientific: London), 1999.

40 Sayari A, Ezzidini M, Azeza B, Rekaya S, Shalaan E, Yaghmour S J, Al-Ghamdi A A, Sfaxi L, M'ghaieth R & Maaref H, *Sol Energy Mater Sol Cells*, 113 (2013) 1.

41 Grundmann M, *Physica E*, 5 (2000) 167.